CERN-FASER-CONF-2026-002
20 March 2026

Cross section measurements of high-energy electron and muon neutrino interactions with FASER's emulsion detector at the LHC

FASER Collaboration

This note presents updated results from the search for high-energy electron and muon neutrino charged-current interactions in the FASERν emulsion/tungsten sub-detector of FASER. A subset of the FASERν volume is used, corresponding to a target mass of 681.1 kg, collecting 9.5 fb^{-1} of LHC proton-proton collision data in 2022 at a centre-of-mass energy of 13.6 TeV. The muon neutrino energy is reconstructed by employing a regression BDT, and the energy dependent cross section is measured in two bins. The electron neutrino cross section is measured in a single bin without energy reconstruction applied.

© 2026 CERN for the benefit of the FASER Collaboration. Reproduction of this article or parts of it is allowed as specified in the CC-BY-4.0 license.

CONTENTS

1. Introduction 1
2. Data Sample 2
3. Event Selection 2
4. Neutrino Energy Reconstruction 4
5. Cross Section Measurement 5
6. Results 7
7. Conclusions 13
A. Cross section plots in linear scale 14
References 16

1. INTRODUCTION

In 2024, the FASER Collaboration reported the first ν_e and ν_μ cross section measurements [1] in the data taken with its second emulsion detector in 2022, corresponding to an integrated luminosity of 9.5 fb^{-1} and a target mass of 128.6 kg. The number of observed events was updated in 2025 [2] using an increased target mass of 314.7 kg.

The current result reports a further update corresponding to a target mass of 681.1 kg, an increase of a factor of 2.2 (5.3) with respect to the 2025 (2024) result. The muon neutrino energy is reconstructed, and the energy dependent cross section for $\nu_\mu + \bar{\nu}_\mu$ is measured in two bins for the first time with the FASER emulsion detector. The cross section for $\nu_e + \bar{\nu}_e$ is measured in a single

bin, without energy reconstruction. The number of candidate events, the energy dependent cross section measurement for ν_μ, and the single bin cross section measurement for ν_e, are presented.

2. DATA SAMPLE

FASER's emulsion detector (FASERν) consists of 730 layers of 1.1 mm thick tungsten plates as the target, interleaved with 0.3 mm thick nuclear emulsion films, acting as trackers. The transverse dimension of each is 25 cm $\times$ 30 cm. The total mass of FASERν is 1.1 tonne. Both the previous and current analyses are conducted on the second module from the 2022 data-taking period, exposed to 9.5 fb^{-1} of data [3]. For readout and processing, each film is divided into "zones" as shown in Fig. 1. Furthermore, for analysis, the data is further divided into small volumes of 1.7 cm $\times$ 1.7 cm $\times$ 30 emulsion films. The data reconstruction process is fully described in the reconstruction paper [4].

The 2024 analysis focused on interactions occurring in zones 3 and 4 across 291 films, extended in the 2025 analysis to include films 8-627 in zones 3–4, and films 8-337 in zones 1-2.

In the present analysis films 8-627 are used for zones 1-6. Films 1–7 are used as a veto for charged parent particles, while 103 films downstream of the target volume are used to identify muons and measure particle momenta via multiple Coulomb scattering (MCS) [1, 5, 6]. The volume covered by the current analysis is illustrated in Fig. 2.

The single-film efficiency is evaluated by checking whether a reconstructed track has a hit in the layer of interest, where the track must have at least four hits among 6 layers, within the ± 3 neighbouring layers from the layer of interest. To ensure consistency with the previous analysis, we restrict the analysis volumes to those in which the single-film efficiency exceeds 80%. In addition to the volume selection described above, fiducial cuts in the XY plane are defined for each zone, as illustrated in Fig. 3. These cuts are determined by an algorithm based on the averaged efficiency threshold of 0.8. The mean of the averaged efficiencies for the selected volumes and within the fiducial regions is found to be 86%.

The detector is aligned with the nominal beam collision axis line-of-sight (LoS), with a transverse dimension large enough to accommodate changes in collision crossing angle in ATLAS. The LoS is a few centimetres away from the centre of the detector, as shown in Fig. 3.

The neutrino target mass is then calculated by selecting good volumes and requiring an overlap of the area with the x-y cut. The analysed target mass is calculated to be 681.1 ± 7 kg, about 2.2 times larger than the previous analysis. This corresponds to 93% of the volume included in the six zones.

3. EVENT SELECTION

Candidate ν_e and ν_μ charged-current (CC) interactions are selected using reconstructed charged-particle tracks that form a neutral vertex in the FASERν detector. In a CC interaction, a high-energy charged lepton and other hadron particles associated with the vertex are back-to-back in the transverse plane.

The event selection follows the same strategy as described in Ref. [1]. The selection is based on reconstructed tracks obtained after multiple steps of alignment and track reconstruction [4]. Vertex reconstruction is performed using tracks passing through at least three plates, selecting converging patterns with an impact parameter below 5 μm and more than four tracks. Tracks must originate within three films downstream of the vertex, and more than three tracks with $\tan\theta \leq 0.1$ are required to suppress the neutral-hadron interaction background, where θ is the polar angle measured from the beam direction. The beam direction is defined by the angular peak

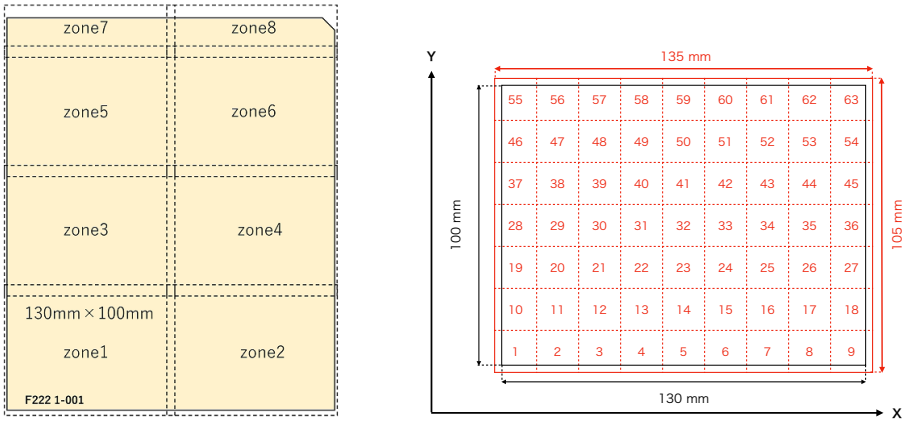


FIG. 1. Left: Definition of zones. The films are divided into eight zones for scanning. To determine the orientation of the films, a small triangular section (∼5 mm) is cut at the top-right corner of each film during production. Right: Division of a scanning zone into 63 overlapping areas, each with 1.7 cm × 1.7 cm size.

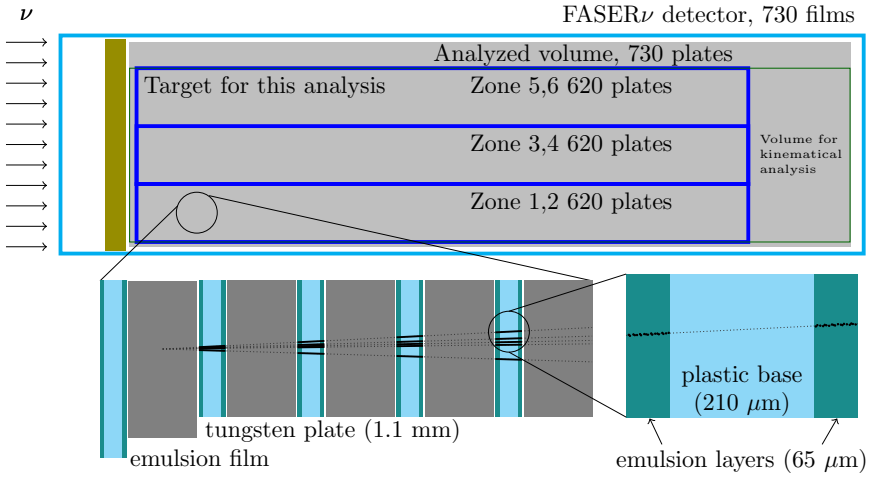


FIG. 2. A schematic illustration of the FASERν emulsion detector.

of background muons measured around each vertex position. A follow-down process for tracks (track follow-down, TFD) [4] is applied to the data sample, extending to 100 plates downstream of each vertex. A reconnection algorithm and an in-track kink search tool are applied to all reconstructed tracks in the TFD volumes.

Candidate ν_e CC interactions are identified by requiring an associated EM shower with energy above 200 GeV and $\tan\theta > 0.005$ to suppress background. Electrons are identified by detecting showering track segments in the emulsion films by opening a cylindrical volume around the candidate track. The EM shower must start within two films downstream of the vertex and have $\Delta\phi > \pi/2$ relative to other vertex-associated tracks, where ϕ is the azimuthal angle in the x-y plane.

Candidate ν_μ CC interactions require at least one muon track, defined as a particle penetrating over 100 tungsten plates without significant secondary interactions. The muon must have momentum above 200 GeV and $\tan\theta > 0.005$. The track must also satisfy $\Delta\phi > \pi/2$.

The selection efficiencies lie approximately between 20 - 40% in the 500 GeV $-$ 2500 GeV range for all flavours. The expected background for ν_e is $0.13^{+0.08}_{-0.05}$ events, and $1.17^{+0.62}_{-0.40}$ events for ν_μ.

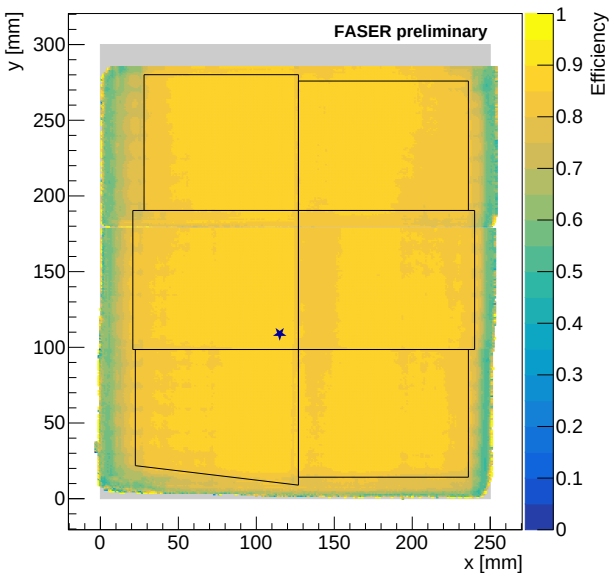


FIG. 3. Fiducial cut (vertex position cut), defined by the averaged efficiency at 0.8. The blue star represents the LoS.

The selection efficiencies and the estimation of backgrounds are further summarised in the previous paper [1].

4. NEUTRINO ENERGY RECONSTRUCTION

Muon neutrino energy is reconstructed from interaction daughter track properties by applying Boosted Decision Trees with gradient boosting (BDTG) to perform a Multivariate Regression Analysis, implemented with the `ROOT TMVA` package [7]. For each event in the training sample, the true neutrino energy E_ν^{truth} is the regression target variable, and the input variables are the daughter muon momentum P_μ, the inverse of the daughter muon angle tangent $1/\tan\theta_\mu$, and the sum of charged hadron momenta $\sum P_{ch.had.}$. The resolution of P_μ is between 20 - 30% below 1 TeV, and 30 - 40% above 1 TeV [5]. Charged hadrons also undergo MCS, and therefore the same tool for momentum measurement is applied. The resolution of θ_μ is 0.067 mrad [4].

The training sample is produced by simulating neutrino interactions within a central region of the FASERν detector to ensure event containment, following a $1/E^2$ incident flux distribution up to 15 TeV, resulting in an approximately flat $dN/d\log E$ distribution of interacting neutrinos across the full energy range of interest.

For each event, the primary daughter tracks are selected from all reconstructed tracks by ensuring that: the first segment of the track lies within 5 plates after the truth neutrino vertex; track momentum is larger than 1 GeV and track $\tan\theta$ is less than 0.5; track has at least 10 segments (number of films with hits in a reconstructed track). After selecting the primary daughter tracks, the events for the training samples are selected by requiring CC events of the correct neutrino flavour, and that the event has at least 1 corresponding daughter lepton track and 1 charged hadron track, both passing the track selections.

Due to shorter tracks lengths of charged hadrons, predominantly due to secondary interactions, $\sum P_{ch.had.}$ has a tendency to underestimate the actual hadronic energy. To correct for this in the training sample, events are selected to only contain tracks which have a reconstructed momentum

of at least 40% of their true momentum. This emulates the effect of the vertexing, reconnection and kink search procedures that are applied to the simulation sample following the neutrino flux prediction and to the data, which greatly reduces the number of incorrectly measured charged hadron momenta. However, statistics in the high energy range are reduced, due to a larger charged track multiplicity and therefore an increase in tracks that may fail the selection. An additional $1/\sqrt{E}$ weighting during training to increase the relative importance of high energy events is added, as it was shown to improve reconstruction performance.

The final training weights for $\nu_\mu + \overline{\nu}_\mu$ events were produced using the combined ν_μ and $\overline{\nu}_\mu$ training samples after applying the event filtering outlined above.

The performance of the energy reconstruction is first evaluated using the testing sample without applying the event selection for neutrinos. The simulation samples are produced as described in Ref. [1]. Fig. 4 shows the correlation of the truth and reconstructed energy. Fig. 5 shows $\Delta E/E$, defined as $(E_\nu^{\text{reco}} - E_\nu^{\text{true}})/E_\nu^{\text{true}}$, as a function of reconstructed energy, in the range 200 GeV - 3 TeV. A good linearity is observed, with the mean of $\Delta E/E$ offset by less than 10% and a resolution in the range of 30 - 40%.

The final performance and the migration between truth and reconstructed neutrino energy are then evaluated using the simulated sample passing the event selection for neutrinos. Fig. 6 shows the correlation of the truth and reconstructed energy, and the subsequent migration matrix of dimensions 3×2.

Sources of systematic uncertainties associated with the input variables are considered in the energy reconstruction. They are evaluated by varying each measured quantity by the systematic uncertainty value (i.e. $x \to x \pm \sigma x$) and applying the TMVA weights to obtain modified migration matrices. The uncertainty contribution from each variable to the neutrino energy reconstruction is found as the difference between the nominal migration matrix and the alternate matrices. The systematic uncertainty of the muon momentum measurement tool from tungsten thickness is estimated to be ±4.5% in Ref. [5]. The uncertainty on the momentum measurement of charged hadron tracks is therefore taken to be the same. Tracks lying in the overflow bin at 7 TeV are not scaled and remain at their overflow value. The sum of charged hadron momenta is then found by summing the scaled track momenta. The resolution of track angle is calculated by summing the resolution of track θ_x, 0.046 mrad, and θ_y, 0.049 mrad, [4] in quadrature, giving 0.067 mrad. The muon angle is scaled by this value, and the inverse of the tangent was calculated. Each source of uncertainty gives less than a 2% shift in the migration matrix.

5. CROSS SECTION MEASUREMENT

We calculate the neutrino cross section directly from the reconstructed neutrino distribution using a Markov chain Monte Carlo (MCMC) method, as performed for the first FASERν measurement [1]. This is implemented using the `emcee` package [8]. The cross section is measured dependent on energy for $\nu_\mu + \bar{\nu}_\mu$, after neutrino energy reconstruction is applied. For the $\nu_e + \bar{\nu}_e$ cross section, it is measured in a single bin without neutrino energy reconstruction.

The expected number of interacting neutrinos is calculated as a function of true differential cross section, σ_i/E_i, assumed constant per energy bin E_i:

$$n_i^{truth}(\sigma_i/E_i) = L\frac{\rho}{m}\frac{\sigma_i}{E_i}\int\int \epsilon_i(E_i)E_i\phi_i(E_i,\vec{x})d\vec{x}dE_i \ , \tag{1}$$

where L is the integrated luminosity, $\frac{\rho}{m}$ is the target density normalised by the nucleon mass ($1.16 \cdot 10^{25}$ cm^{-3}), $\epsilon_i(E_i)$ is the detection efficiency, and $\int \phi_i(E_i,\vec{x})d\vec{x}$ is the predicted incident

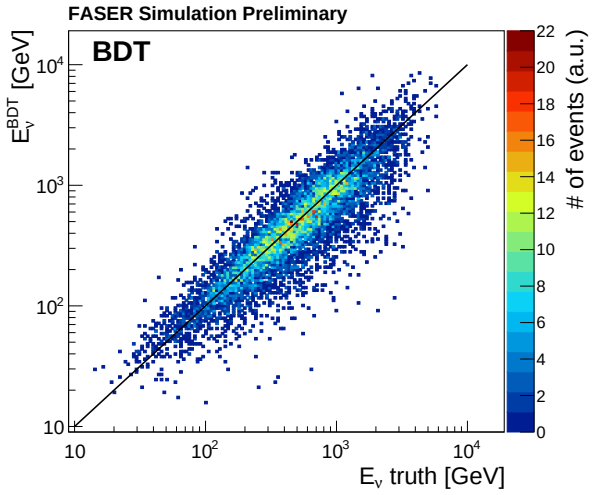


FIG. 4. Reconstructed energy against true neutrino energy after applying the trained BDT on the test sample, calculated without the event selections in Sec. 3

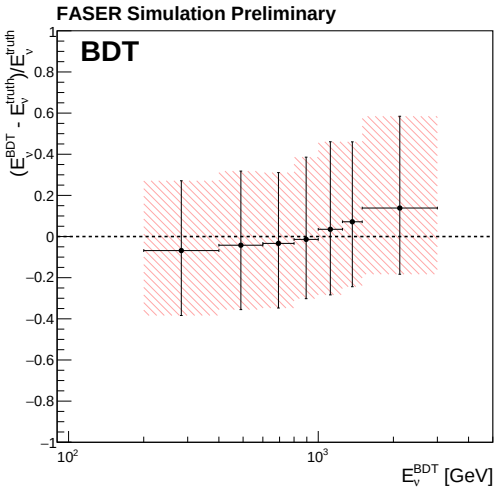
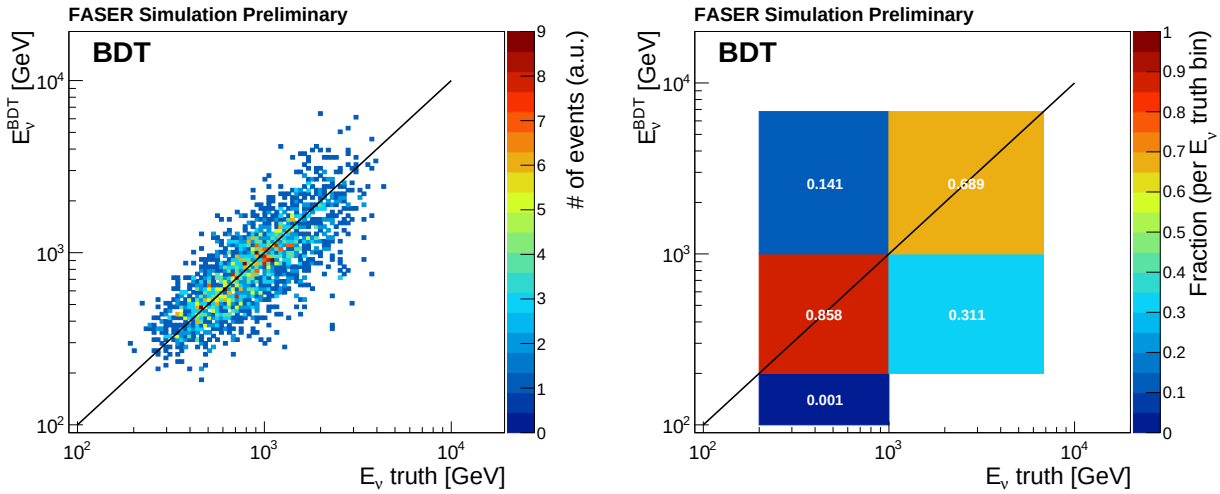


FIG. 5. $\Delta E/E$ as a function of reconstructed energy, in the range of 200 GeV to 3 TeV. The central values are the 50th percentile, and the vertical error bars show the range between the 16th and 84th percentiles.



(a) (b)

FIG. 6. (a) The correlation of the truth and reconstructed energy using the test sample after applying event selections. (b) The migration matrix for the sample after applying event selections.

neutrino flux integrated over area (cm^2). All terms other than σ_i/E_i are calculated using flux estimates and efficiency.

For muon neutrino events, the expected number of observed events in reconstructed energy bins E_j can be calculated by applying the migration matrix $\boldsymbol{M}$ from the neutrino energy reconstruction tool described in Sec. 4 (Fig. 6(b)) to $n_i^{truth}(\sigma_i/E_i)$, and adding background terms n_b^{bkg}:

$$n_j^{\nu_\mu,reco}(\sigma_j/E_j) = \sum_i M_{ji} n_i^{\nu_\mu,truth}(\sigma_i/E_i) + \sum_b n_{b,j}^{bkg} \ ; \tag{2}$$

where i sums over true energy bins E_i, and b sums over sources of background.

For electron neutrino events, no energy reconstruction is performed and no migration matrix is applied. This is due to limited statistics for a multi-binned analysis. The expected number of observed events in a single energy bin E_j is therefore:

$$n_j^{\nu_e,reco}(\sigma_j/E_j) = n_j^{\nu_e,truth}(\sigma_j/E_j) + \sum_b n_{b,j}^{bkg} \ . \tag{3}$$

The likelihood is defined as

$$\mathcal{L} = \prod_j (P(N_j^{reco} \mid n_j^{reco}(\sigma_j/E_j)) \cdot \prod_k G(\theta_{k,j})) \ ; \tag{4}$$

where $P(N_j^{reco} \mid n_j^{reco}(\sigma_j/E_j))$ is the Poisson probability of observing N_j^{reco} events given the expectation of n_j^{reco} events in bin E_j, and $G(\theta_{k,j})$ denotes the Gaussian priors of the nuisance parameters θ_k, per source of uncertainty k.

Uncertainties on the migration matrix are considered by converting $M_{ji} \rightarrow M_{ji} + \sum_m \theta_m \sigma_{M_{ji},m}$, where $\sigma_{M_{ji},m}$ terms are matrices of the absolute differences between the nominal migration matrix and the matrices produced by scaling the systematic uncertainties on reconstructed energy by $\pm 1\sigma$. The uncertainties are assumed to be fully correlated between energy bins, and a single nuisance parameter is used for each source.

All other uncertainties are considered by converting:

$$n_i^{truth}(\sigma_i/E_i) \rightarrow n_i^{truth}(\sigma_i/E_i) \ \cdot \prod_p (1 + \theta_p \sigma_p^{corr.}) \ \cdot \prod_{q,i} (1 + \theta_{q,i} \sigma_{q,i}^{uncorr.}) \ ; \tag{5}$$

where $\prod_{q,i}(1 + \theta_i \sigma_{q,i}^{uncorr.})$ is the product of uncorrelated uncertainties q, and $\prod_p (1 + \theta \sigma_p^{corr.})$ is the product of correlated uncertainties p.

The MCMC iterates over 53000 steps, rejecting the first 3000 for initialisation, and provides the probability distribution function (PDF) for each cross section measured. The measured value for each cross section is taken as the mean of the PDF, and the associated uncertainties are taken as the 16th and 84th percentiles of the PDF.

6. RESULTS

The number of observed ν_e CC and ν_μ CC candidate events are summarised in Table 1. Example event displays of ν_e and ν_μ candidates are shown in Fig. 7. As expected, both events exhibit a back-to-back topology between the lepton candidate and the other tracks in the vertex. The positions of the selected vertices in the transverse and longitudinal planes are shown in Fig. 8.

Seven events are selected by the ν_e selection on data. The properties of the selected vertices are compared with the expectations from ν_e CC simulation (Fig. 9). The simulation samples are described in Ref. [1]. It is based on GENIE, and the flux predictions described in Ref. [9] are used. Two additional candidates were found in the sample from the added target mass.

TABLE 1. Summary of the selected events, including the candidate events reported in Ref. [1]. The flux predictions described in Ref. [9] are used.

	ν_e CC	ν_μ CC
Expected signal	$7.7^{+6.3}_{-2.5}$	$40.0^{+14.5}_{-9.7}$
Expected background	$0.13^{+0.08}_{-0.05}$	$1.17^{+0.62}_{-0.40}$
Observed events	7	33

In total 33 events are selected by the ν_μ selection on data. The properties of these selected vertices are compared with the expectation from ν_μ CC simulation (Fig. 10). An additional 13 candidates were found in the sample from the added target mass.

More details about the properties of the individual tracks forming the vertices can be found in [10]. In general, the simulation describes the data well for both the ν_e and ν_μ selections. The expected number of neutrino signal events satisfying the selections are in the range 5.2–14.0 for ν_e CC and 30.3–54.5 for ν_μ CC, where the range covers the uncertainties reported in Ref. [1]. Flux and selection efficiency uncertainties dominate. The observed number of interactions is consistent with Standard Model predictions.

The energy of the muon neutrino candidates is reconstructed using the method described in Sec. 4, and the events are binned following the migration matrix in Fig. 6(b). In the reconstructed energy range of 200 GeV − 1000 GeV, 19 events were observed, and 14 events were observed with a reconstructed energy > 1000 GeV. Table 2 and Fig. 11 show the binned number of observed neutrinos compared to the expected true and the expected observed (reconstructed + background) number of neutrinos from flux and efficiency estimates. Fig. 12 shows, in finer bins, the observed neutrino events compared to the expected number of events from MC scaled to luminosity and target mass. The highest reconstructed muon neutrino energy from the selected ν_μ CC candidates is 2.95 TeV, with $P_\mu = 1.58$ TeV.

The energy dependent cross section is calculated in two bins following the method described in Sec. 5. The measured cross section is calculated as $0.32^{+0.17}_{-0.18}$ $\times 10^{-38}$ cm^2 GeV^{-1} (stat.) and $0.32^{+0.18}_{-0.18}$ $\times 10^{-38}$ cm^2 GeV^{-1} (stat. + syst.) in the neutrino energy range 200 GeV − 1000 GeV, and $0.55^{+0.22}_{-0.21}$ $\times 10^{-38}$ cm^2 GeV^{-1} (stat.) and $0.55^{+0.24}_{-0.25}$ $\times 10^{-38}$ cm^2 GeV^{-1} (stat. + syst.) for neutrinos with energy > 1000 GeV. The measured cross section is shown in Fig. 13, along with the predicted theoretical cross section and previous experimental results [11–33]. The lower bin centre is calculated as the log centre of the range, 447 GeV. The upper bin centre is defined as the mean of the reconstructed neutrino distribution, using baseline models, that fall in the range, 1483 GeV. The upper bin edge is defined as as the 95th percentile of the distribution, 3129 GeV. The statistical uncertainty dominates. Among the systematic uncertainties, the leading sources (depending on the bin) are the selection efficiency uncertainty due to the hadronisation in neutrino interactions in simulation (15 - 29%), and the selection efficiency uncertainty from reconstruction (20%), followed by the flux uncertainty on light hadron production (10 - 22%).

The electron neutrino cross section is measured in a single bin without energy reconstruction, following the method described in Sec. 5. The measured cross section is calculated as $0.43^{+0.17}_{-0.17}$ $\times 10^{-38}$ cm^2 GeV^{-1} (stat.) and $0.43^{+0.22}_{-0.23}$ $\times 10^{-38}$ cm^2 GeV^{-1} (stat. + syst.) The measured cross section is shown in Fig. 14, along with the predicted theoretical cross section and previous experimental results [34, 35]. The energy range displayed is defined to contain the central 68% of reconstructed neutrinos using baseline models, which is 553 GeV − 1670 GeV, with the central point marking the 50th percentile of the distribution, corresponding to 950 GeV. The sta-

tistical uncertainty dominates. Among the systematic uncertainties, the leading source is the flux uncertainty on charm hadron production (65%), followed by the the selection efficiency uncertainty due to the hadronisation in neutrino interactions in simulation (22%).

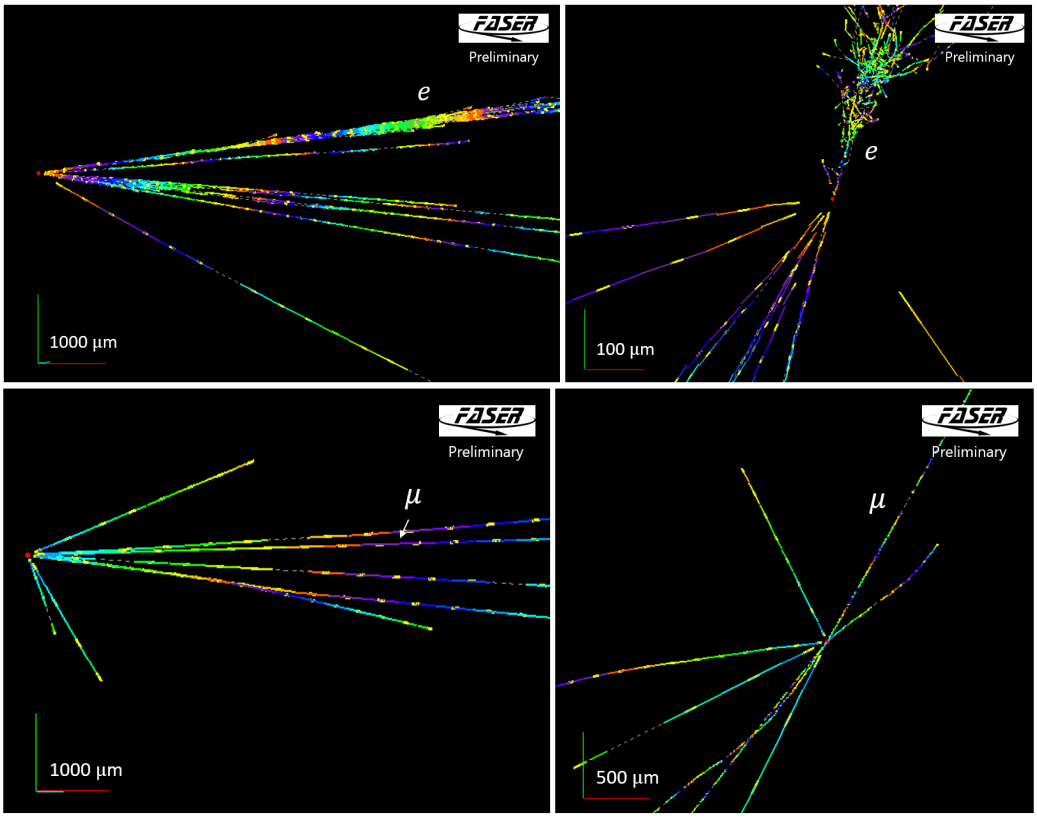


FIG. 7. Event displays of one of the ν_e CC candidate events (top) and one of the ν_μ CC candidate events (bottom) detected in the newly analysed volume. In each panel, the right-handed coordinate axes are shown in the bottom left, with red, green, and blue axes indicating the x (horizontal), y (vertical), and z (beam) directions, respectively. The left panels are slightly rotated views to show the longitudinal development of the event. The right panels show views transverse to the beam direction, and so the blue axes are not visible. Yellow line segments show the trajectories of charged particles in the emulsion films. The other coloured lines are interpolations, with the colours indicating the longitudinal depth in the detector. The ν_e CC candidate event has an electron energy of 465 GeV. The ν_μ CC candidate event has a reconstructed neutrino energy of 767 GeV, with $P_\mu = 539$ GeV, $\sum P_{ch.had.} = 189$ GeV, and $\tan\theta_\mu$ of 0.023.

TABLE 2. The expected number of observed muon neutrino events in each bin for truth MC and reconstructed MC with background (flux predictions described in Ref. [9] and efficiencies from Ref. [1] are used), and the observed number of muon neutrino events in data.

Reconstructed E_ν bin (GeV)	$10-200$	$200-1000$	>1000
n_{exp}^{truth}	$0.00^{+0.00}_{-0.00}$	$22.3^{+8.4}_{-5.4}$	$17.9^{+7.0}_{-4.7}$
$n_{exp}^{reco} = (\boldsymbol{M} \times n_{exp}^{truth}) + n_{exp}^{bkg}$	$0.02^{+0.01}_{-0.00}$	$25.8^{+9.0}_{-6.1}$	$15.5^{+5.8}_{-4.0}$
N_{obs}^{reco}	0	19	14

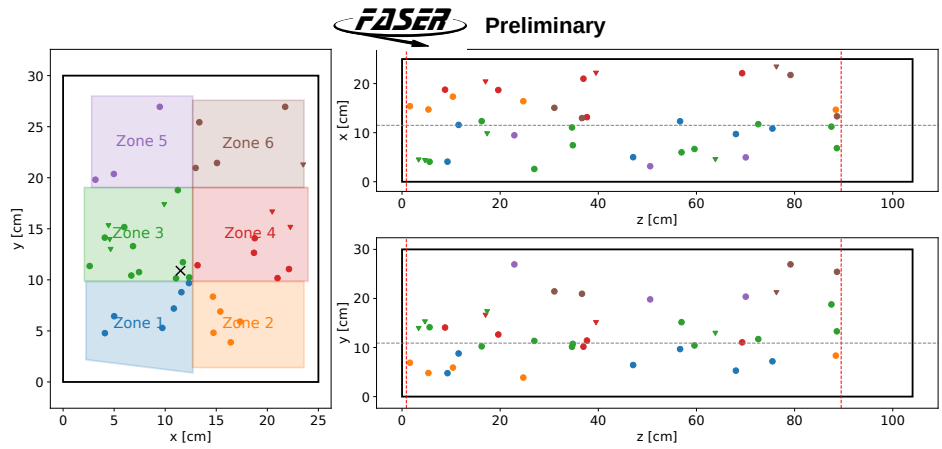


FIG. 8. Vertex positions in the transverse (xy) and longitudinal (xz, yz) planes of the observed ν_e CC (triangles) and ν_μ CC (circles) candidate events in the data sample. The nominal LoS is marked by the $\times$ in the transverse plane, and the grey dashed line in the longitudinal planes. The uncertainty in the LoS position is about 1 cm. Coloured polygons show the transverse fiducial volume cuts for each detector zone, and the red dashed lines indicate the longitudinal fiducial cuts.

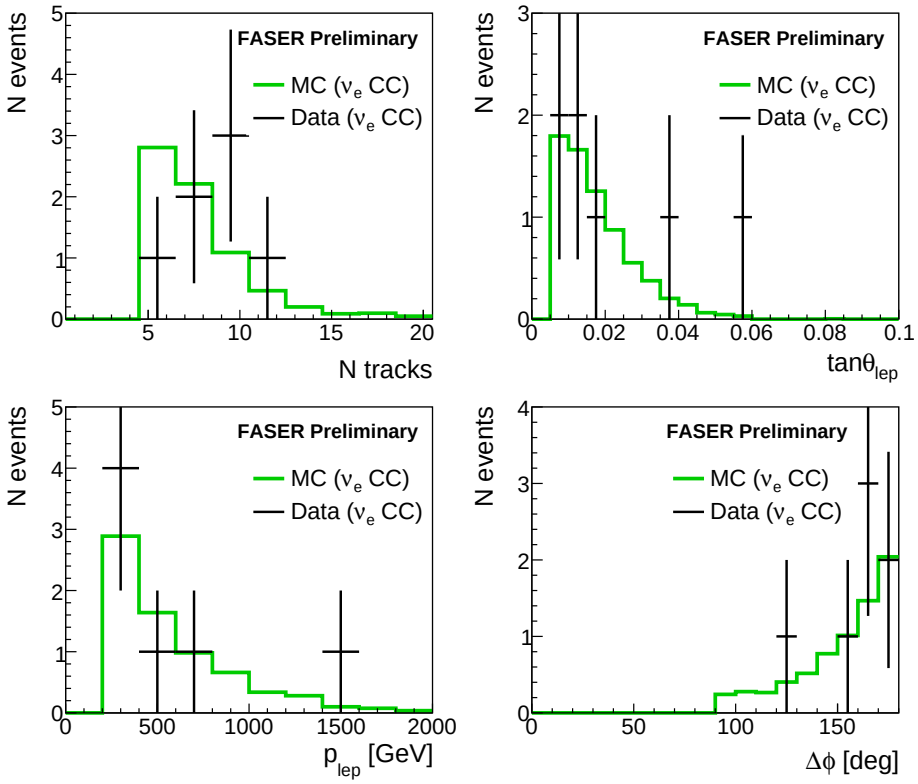


FIG. 9. MC simulation distributions of the track multiplicity (N tracks), lepton angle ($\tan\theta_{\rm lep}$), lepton momentum ($p_{\rm lep}$), and $\Delta\phi$ for the ν_e CC signal that passed the selection criteria. The observed ν_e CC candidate events in the data sample are shown in black. The MC simulation distributions are normalised to the number of observed events.

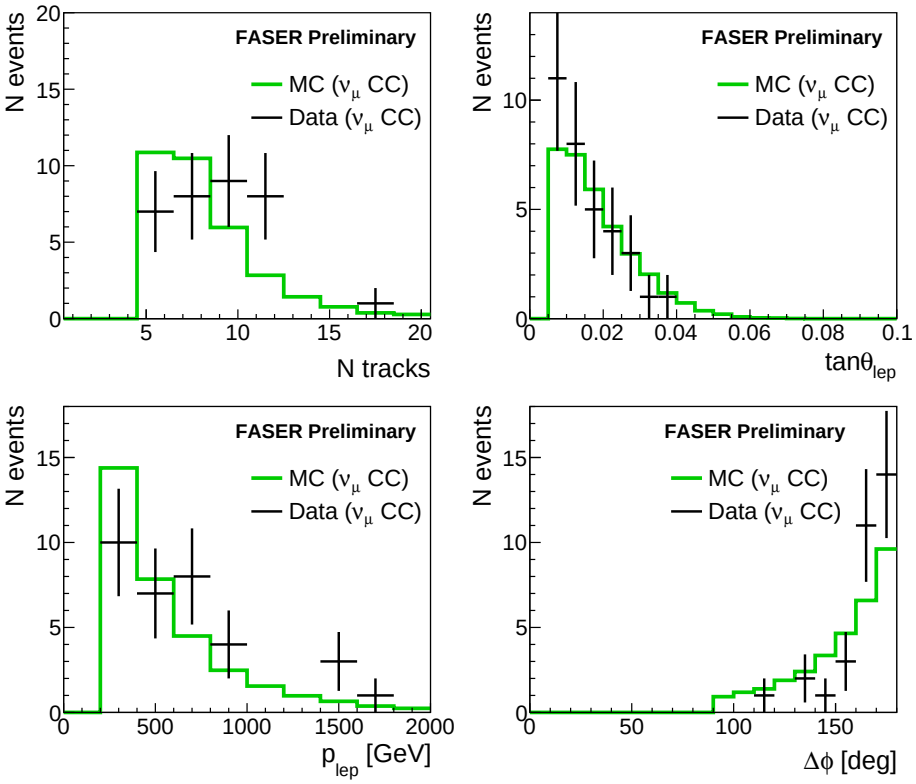


FIG. 10. MC simulation distributions of the track multiplicity (N tracks), lepton angle ($\tan\theta_{\rm lep}$), lepton momentum ($p_{\rm lep}$), and $\Delta\phi$ for the ν_μ CC signal that passed the selection criteria. The observed ν_μ CC candidate events in the data sample are shown in black. The MC simulation distributions are normalised to the number of observed events.

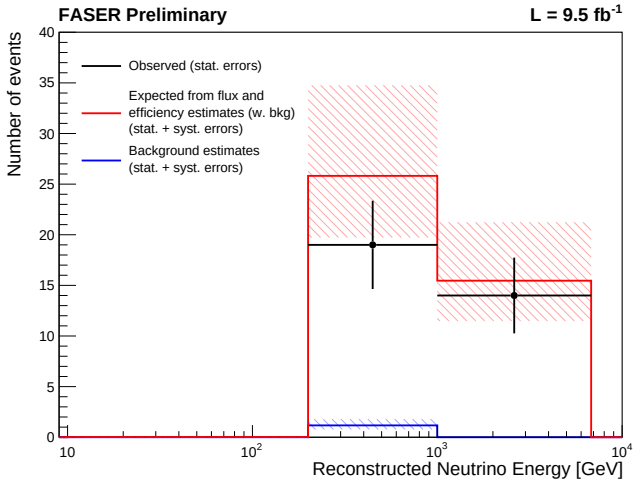


FIG. 11. The energy distribution of the observed muon neutrino events with the statistical uncertainty on the observation (black), compared to the expected energy distribution of observed muon neutrino events (red), calculated from flux and efficiency estimates, including background contributions (blue), with statistical and systematic uncertainties (hashed areas), corresponding to the values shown in Table 2.

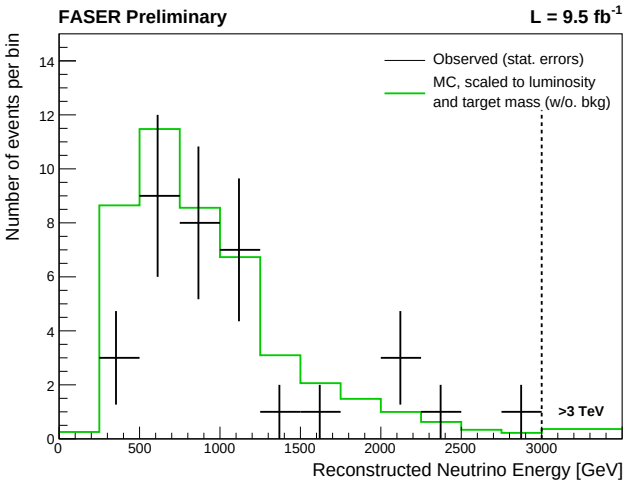


FIG. 12. The energy distribution of the observed muon neutrino events with the statistical uncertainty on the observation (black), compared to the expected energy distribution of observed muon neutrino events (green) from MC scaled to luminosity and target mass, without background.

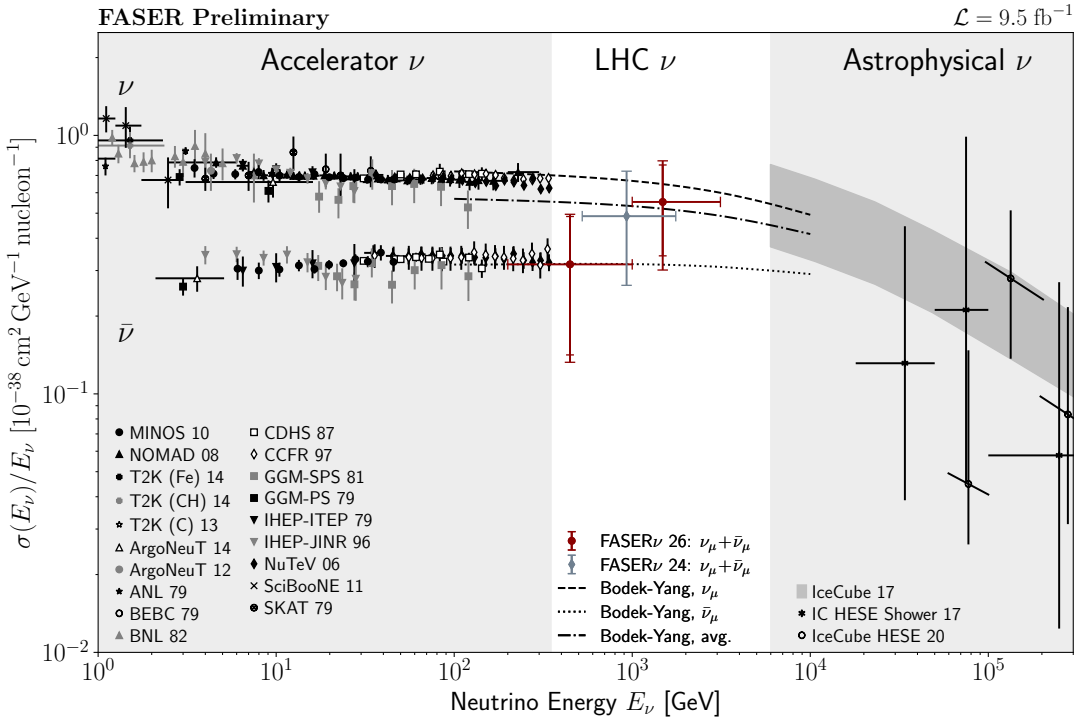


FIG. 13. The CC muon neutrino cross section divided by energy, measured in two neutrino energy bins (200 GeV − 1000 GeV, > 1000 GeV), using data from second FASER emulsion module of 2022. The lower bin centre is calculated as the log centre of the range, 447 GeV. The upper bin centre is defined as the mean of the reconstructed neutrino distribution, using baseline models, that fall in the range, 1483 GeV. The upper bin edge is defined as as the 95th percentile of the distribution, 3129 GeV.

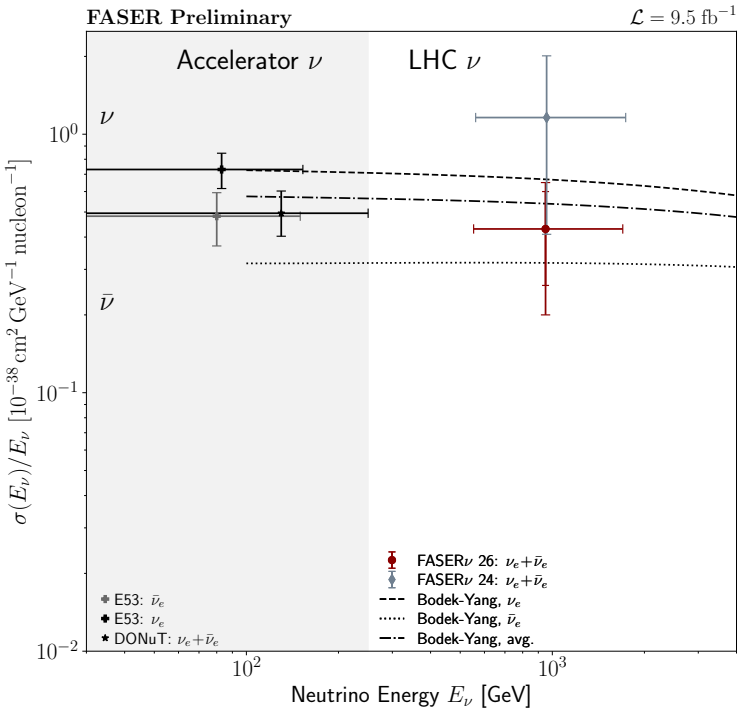


FIG. 14. The CC electron neutrino cross section divided by energy, measured in a single bin, using data from the second FASER emulsion module of 2022. The inner error bars show the statistical uncertainty, and the outer error bars show the combined statistical and systematic uncertainties. The energy range displayed is defined to contain the central 68% of reconstructed neutrinos using baseline models, which is 553 GeV − 1670 GeV, with the central point marking the 50th percentile of the distribution, corresponding to 950 GeV.

7. CONCLUSIONS

Updated results of the high-energy electron and muon neutrino interactions in the FASERν tungsten/emulsion detector of the FASER experiment have been presented. Seven electron-neutrino interaction candidate events and thirty three muon-neutrino interaction candidate events are observed in 9.5 fb^{-1} of data with a target mass of 681.1 kg.

The muon neutrino energy is reconstructed, and the energy dependent cross section is measured in two bins to be $0.32^{+0.18}_{-0.18}$ $\times 10^{-38}$ cm^2 GeV^{-1} in the range 200 GeV − 1000 GeV and $0.55^{+0.24}_{-0.25}$ $\times 10^{-38}$ cm^2 GeV^{-1} above 1000 GeV. The electron neutrino cross section is measured in a single bin, without energy reconstruction, to be $0.43^{+0.22}_{-0.23}$ $\times 10^{-38}$ cm^2 GeV^{-1} .

The muon and electron neutrino cross section measurements are consistent with previous FASER results within experimental uncertainties, both for analyses using the electronic detector (ν_μ) [36] and emulsion detector (ν_μ, ν_e) [1].

This analysis represents progress toward an extensive physics program focused on neutrino studies, offering valuable understanding not only of neutrino and electroweak physics, but also of quantum chromodynamics through the investigation of forward hadron production and deep inelastic scattering involving high-energy neutrinos.

Appendix A: Cross section plots in linear scale

The plots in this section, Fig. 15 and Fig. 16, are identical to Fig. 13 and Fig. 14, respectively, but plotted with a linear y-axis scale.

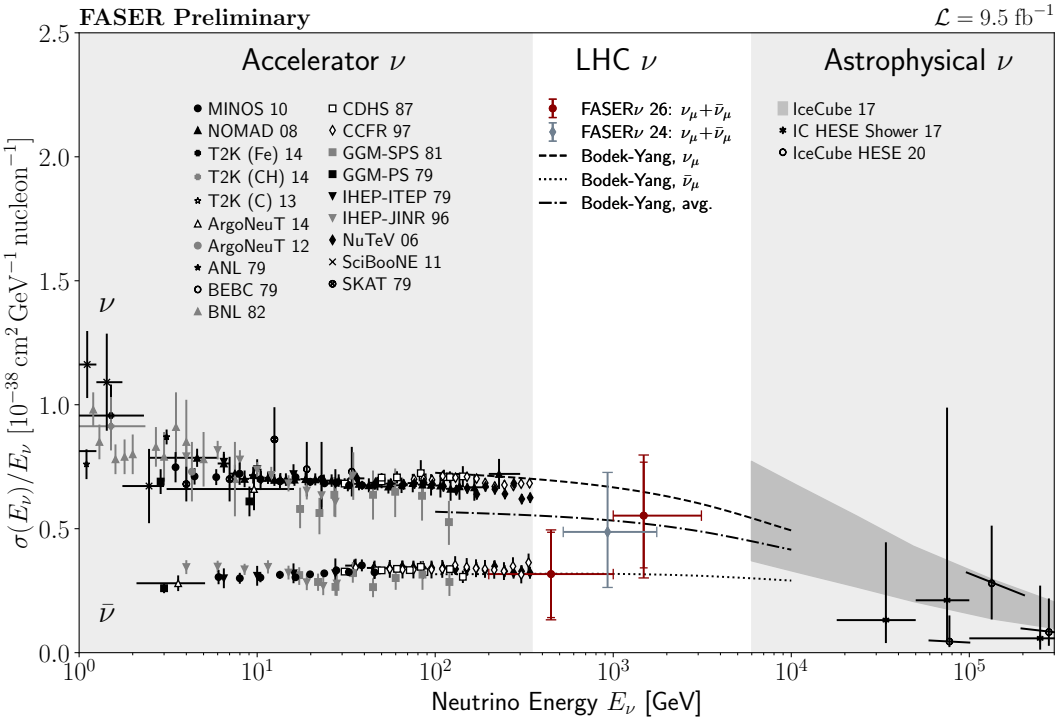


FIG. 15. Same as Fig. 13, with a linear y-axis scale.

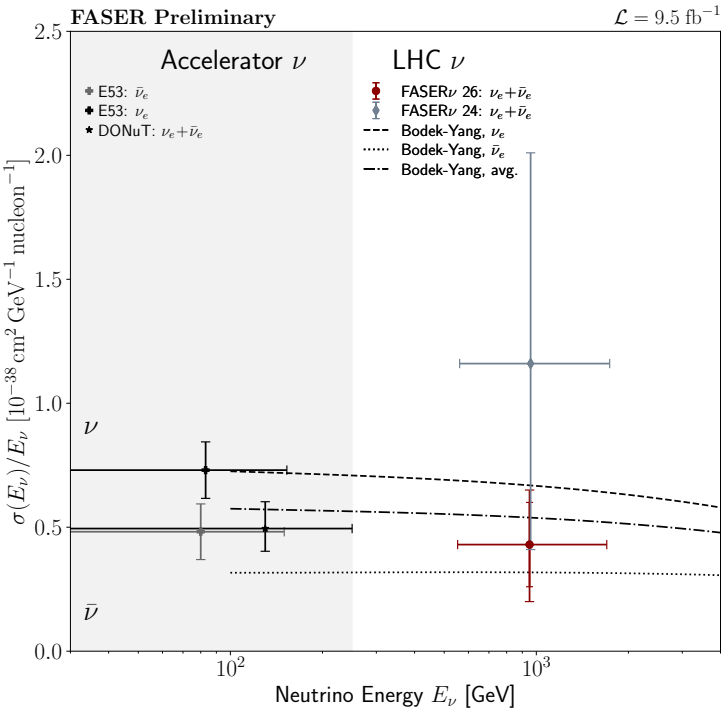


FIG. 16. Same as Fig. 14, with a linear y-axis scale.

[1] **FASER** Collaboration, "First Measurement of ν_e and ν_μ Interaction Cross Sections at the LHC with FASER's Emulsion Detector," *Phys. Rev. Lett.* **133** (2024) no. 2, 021802, arXiv:2403.12520 [hep-ex].

[2] **FASER** Collaboration, "Updated results of high-energy electron and muon neutrino interactions with FASER's emulsion detector at the LHC," CERN-FASER-CONF-2025-002. https://cds.cern.ch/record/2927714.

[3] **ATLAS** Collaboration, "Luminosity determination in pp collisions at $\sqrt{s} = 13$ TeV using the ATLAS detector at the LHC," *Eur. Phys. J. C* **83** (2023) no. 10, 982, arXiv:2212.09379 [hep-ex].

[4] **FASER** Collaboration, "Reconstruction and performance evaluation of FASER's emulsion detector at the LHC," *JINST* **20** (2025) no. 12, P12018, arXiv:2504.13008 [physics.ins-det].

[5] **FASER** Collaboration, "Momentum Measurement of Charged Particles in FASER's Emulsion Detector at the LHC," arXiv:2602.17575 [physics.ins-det].

[6] **FASER** Collaboration, "Detecting and Studying High-Energy Collider Neutrinos with FASER at the LHC," *Eur. Phys. J. C* **80** (2020) no. 1, 61, arXiv:1908.02310 [hep-ex].

[7] **TMVA** Collaboration, A. Hocker *et al.*, "TMVA - Toolkit for Multivariate Data Analysis," arXiv:physics/0703039.

[8] D. Foreman-Mackey, D. W. Hogg, D. Lang, and J. Goodman, "emcee: The MCMC Hammer," *Publ. Astron. Soc. Pac.* **125** (2013) 306–312, arXiv:1202.3665 [astro-ph.IM].

[9] **FASER** Collaboration, "Neutrino Rate Predictions for FASER," *Phys. Rev. D* **110** (2024) no. 1, 012009, arXiv:2402.13318 [hep-ex].

[10] **FASER** Collaboration, "First search for neutrino production of charm hadrons with FASER's emulsion detector at the LHC," CERN-FASER-CONF-2026-003. https://cds.cern.ch/record/2956186.

[11] **MINOS** Collaboration, P. Adamson *et al.*, "Neutrino and Antineutrino Inclusive Charged-current Cross Section Measurements with the MINOS Near Detector," *Phys. Rev. D* **81** (2010) 072002, arXiv:0910.2201 [hep-ex].

[12] **NOMAD** Collaboration, Q. Wu *et al.*, "A Precise measurement of the muon neutrino-nucleon inclusive charged current cross-section off an isoscalar target in the energy range $2.5 < \mathrm{E}_\nu < 40$-GeV by NOMAD," *Phys. Lett. B* **660** (2008) 19–25, arXiv:0711.1183 [hep-ex].

[13] **T2K** Collaboration, K. Abe *et al.*, "Measurement of the inclusive ν_μ charged current cross section on carbon in the near detector of the T2K experiment," *Phys. Rev. D* **87** (2013) no. 9, 092003, arXiv:1302.4908 [hep-ex].

[14] **T2K** Collaboration, K. Abe *et al.*, "Measurement of the ν_μ charged-current quasielastic cross section on carbon with the ND280 detector at T2K," *Phys. Rev. D* **92** (2015) no. 11, 112003, arXiv:1411.6264 [hep-ex].

[15] **T2K** Collaboration, K. Abe *et al.*, "Measurement of the inclusive ν_μ charged current cross section on iron and hydrocarbon in the T2K on-axis neutrino beam," *Phys. Rev. D* **90** (2014) no. 5, 052010, arXiv:1407.4256 [hep-ex].

[16] **ArgoNeuT** Collaboration, C. Anderson *et al.*, "First Measurements of Inclusive Muon Neutrino Charged Current Differential Cross Sections on Argon," *Phys. Rev. Lett.* **108** (2012) 161802, arXiv:1111.0103 [hep-ex].

[17] **ArgoNeuT** Collaboration, R. Acciarri *et al.*, "Measurements of Inclusive Muon Neutrino and Antineutrino Charged Current Differential Cross Sections on Argon in the NuMI Antineutrino Beam," *Phys. Rev. D* **89** (2014) no. 11, 112003, arXiv:1404.4809 [hep-ex].

[18] S. J. Barish *et al.*, "Study of Neutrino Interactions in Hydrogen and Deuterium: Inelastic Charged Current Reactions," *Phys. Rev. D* **19** (1979) 2521.

[19] J. G. H. de Groot *et al.*, "Inclusive Interactions of High-Energy Neutrinos and anti-neutrinos in Iron," *Z. Phys. C* **1** (1979) 143.

[20] D. C. Colley *et al.*, "Cross-sections for Charged Current Neutrino and Anti-neutrino Interactions in the Energy Range 10-GeV to 50-GeV," *Z. Phys. C* **2** (1979) 187.

[21] N. J. Baker, P. L. Connolly, S. A. Kahn, M. J. Murtagh, R. B. Palmer, N. P. Samios, and M. Tanaka, "Total Cross-sections for Muon-neutrino N and Muon-neutrino P Charged Current Interactions in the 7-ft Bubble Chamber," *Phys. Rev. D* **25** (1982) 617–623.

[22] J. P. Berge *et al.*, "Total Neutrino and Anti-neutrino Charged Current Cross-section Measurements in 100-GeV, 160-GeV and 200-GeV Narrow Band Beams," *Z. Phys. C* **35** (1987) 443.

[23] W. G. Seligman, *A Next-to-Leading Order QCD Analysis of Neutrino - Iron Structure Functions at the Tevatron*. PhD thesis, Nevis Labs, Columbia U., 1997.

[24] **Gargamelle Neutrino Propane, Aachen-Brussels-CERN-Ecole Poly-Orsay-Padua** Collaboration, S. Ciampolillo *et al.*, "Total Cross-section for Neutrino Charged Current Interactions at 3-GeV and 9-GeV," *Phys. Lett. B* **84** (1979) 281–284.

[25] **Gargamelle SPS** Collaboration, J. G. Morfin *et al.*, "Total Cross-sections and Nucleon Structure Functions in the Gargamelle SPS Neutrino / Anti-neutrino Experiment," *Phys. Lett. B* **104** (1981) 235–238.

[26] A. I. Mukhin, V. F. Perelygin, K. E. Shestermanov, A. A. Volkov, A. S. Vovenko, and V. P. Zhigunov, "Energy Dependence of Total Cross-sections for Neutrino and Anti-neutrino Interactions at Energies Below 35-GeV," *Sov. J. Nucl. Phys.* **30** (1979) 528.

[27] V. B. Anikeev *et al.*, "Total cross-section measurements for muon-neutrino, anti-muon-neutrino interactions in 3-GeV - 30-GeV energy range with IHEP-JINR neutrino detector," *Z. Phys. C* **70** (1996) 39–46.

[28] **NuTeV** Collaboration, M. Tzanov *et al.*, "Precise measurement of neutrino and anti-neutrino differential cross sections," *Phys. Rev. D* **74** (2006) 012008, arXiv:hep-ex/0509010.

[29] **SciBooNE** Collaboration, Y. Nakajima *et al.*, "Measurement of Inclusive Charged Current Interactions on Carbon in a Few-GeV Neutrino Beam," *Phys. Rev. D* **83** (2011) 012005, arXiv:1011.2131 [hep-ex].

[30] D. S. Baranov *et al.*, "Measurements of the $\nu_\mu N$ Total Cross-section at 2-GeV - 30-GeV in Skat Neutrino Experiment," *Phys. Lett. B* **81** (1979) 255–257.

[31] **IceCube** Collaboration, M. G. Aartsen *et al.*, "Measurement of the multi-TeV neutrino cross section with IceCube using Earth absorption," *Nature* **551** (2017) 596–600, arXiv:1711.08119 [hep-ex].

[32] M. Bustamante and A. Connolly, "Extracting the Energy-Dependent Neutrino-Nucleon Cross Section above 10 TeV Using IceCube Showers," *Phys. Rev. Lett.* **122** (2019) no. 4, 041101, arXiv:1711.11043 [astro-ph.HE].

[33] **IceCube** Collaboration, R. Abbasi *et al.*, "Measurement of the high-energy all-flavor neutrino-nucleon cross section with IceCube," *Phys. Rev. D* **104** (2021) no. 2, 022001, arXiv:2011.03560 [hep-ex].

[34] C. Baltay *et al.*, "$\nu_\mu - \nu_e$ Universality in Charged Current Neutrino Interactions," *Phys. Rev. D* **41** (1990) 2653.

[35] **DONuT** Collaboration, K. Kodama *et al.*, "Final tau-neutrino results from the DONuT experiment," *Phys. Rev. D* **78** (2008) 052002, arXiv:0711.0728 [hep-ex].

[36] **FASER** Collaboration, "First Measurement of the Muon Neutrino Interaction Cross Section and Flux as a Function of Energy at the LHC with FASER," *Phys. Rev. Lett.* **134** (2025) no. 21, 211801, arXiv:2412.03186 [hep-ex].